ACS Photonics

pubs.acs.org/journal/apchd5

Article

Bound States in the Continuum Help Shrimp Eyes to Catch More Light

Andrey Machnev, Daniel Ofer, Hod Gilad, Jenia Binenbaum, Lior Schneidman, Ya'arit Levitt-Barmats, Pavel Ginzburg, and Roman E. Noskov*

Cite This: *ACS Photonics* 2023, 10, 179−184

Read Online

ACCESS | Metrics & More | Article Recommendations | Supporting Information

ABSTRACT: Optical bound states in the continuum (BICs) have recently attracted a great deal of attention as an efficient way to localize and manipulate light at nanoscale. Traditionally, generation of BICs has relied on using artificial structures where suppression of radiative losses leads to very high Q factors. Here, we show that BICs may play an important biological role by boosting light−matter interactions in a biogenic nanostructure: tapetum reflector of a shrimp eye. Enveloping photosensitive units of the retina (rhabdoms), this system contains quasi-periodic arrays of spherical core−shell nanoparticles which include concentric lamellae of single-crystal isoxanthopterin nanoplates arranged around a hollow core. The radial alignment of the plates gives rise to the spherical anisotropy of the nanoparticles which provides access to quasi-BIC modes in a full visible domain. Thus, a tapetum reflector hosting BICs maximizes light interactions with rhabdoms, enhancing the eye's sensitivity. Our findings suggest that BICs, previously associated with man-made structures only, can be generated in biogenic structures, performing crucial optical functionalities in living organisms.

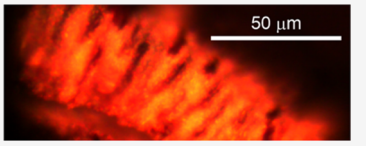

KEYWORDS: *all-dielectric nanophotonics, biogenic structures, spherulites, multipole expansion, isoxanthopterin*

INTRODUCTION

Some animals employ mirrors instead of lenses for vision.[1] Specifically, this approach is common in aquatic environments, where the efficiency of conventional lens-based eyes dramatically drops due to the reduced refractive index contrast between the outside media and the cornea. For example, the eyes of shrimps, lobsters, crayfish, and prawns are composed of thousands of square-faceted eye units (ommatidia) that form images through reflective optics.[2] Figure 1a shows the principle of light collection by such eyes. Distal mirrors placed in the upper part of the eye reflect incoming light onto the photosensitive elements of the retina, the rhabdoms. The tapetum, enveloping the retina, acts as a second reflector that scatters the photons that were not absorbed by rhabdoms on the first pass back into the retina to enhance the light collection efficiency. This is especially important to see in dimmer light and to prevent cross-talk between adjacent rhabdoms in the retina.[3] Typically, high tapetum reflectivity is based on the interference principles of thin-film optics when various pigments or biogenic crystals of guanin or cellulose form iridescent nanolayers, acting as Bragg mirrors.[1]

Recently, a novel type of the tapetum organization was revealed. The tapetum of decapod crustaceans contains quasi-periodic arrays of core−shell nanoparticles composed of a previously unknown biogenic crystal—the pteridine isoxanthopterin.[3,4] The shell of the nanoparticles is formed from concentric lamellae—many single-crystal isoxanthopterin nanoplates radially oriented around a hollow core. Such spatial arrangement of isoxanthopterin nanoplates along with their intrinsic birefringence gives rise to a radial-type dielectric anisotropy of the nanoparticles. Although it was proposed that the main role of this radial anisotropy is to broaden the spectral range for the tapetum reflectivity in comparison with an isotropic case,[4] the physical mechanism standing behind optical functionalities of such a tapetum structure has not been fully understood yet.

Bound states in the continuum (BICs) were first introduced in quantum mechanics as electron waves that remain localized, even though they coexist with a continuous spectrum of radiating modes that can carry energy away.[5] Being a general wave phenomenon,[6] BICs have recently attracted considerable attention in photonics.[7−10] So-called true or symmetry-protected BIC is formed when the mode of one symmetry class is embedded in the continuum of another symmetry class so that the vanishing interaction between them gives rise to an infinite Q factor. True BICs, however, can exist only in ideal, lossless, infinite structures.[11−13] In practice, BICs manifest themselves as quasi-BICs (Q-BICs) with a large but finite Q factor restricted by coupling with radiation and absorption loss channels via a finite sample size, material absorption, inhomogeneous excitation, and structural imperfections.[13] Until now, BICs have been observed only for man-made structures, including photonic crystals, hollow-core photonic

Received: September 12, 2022
Published: December 21, 2022

https://doi.org/10.1021/acsphotonics.2c01429
ACS Photonics 2023, 10, 179−184

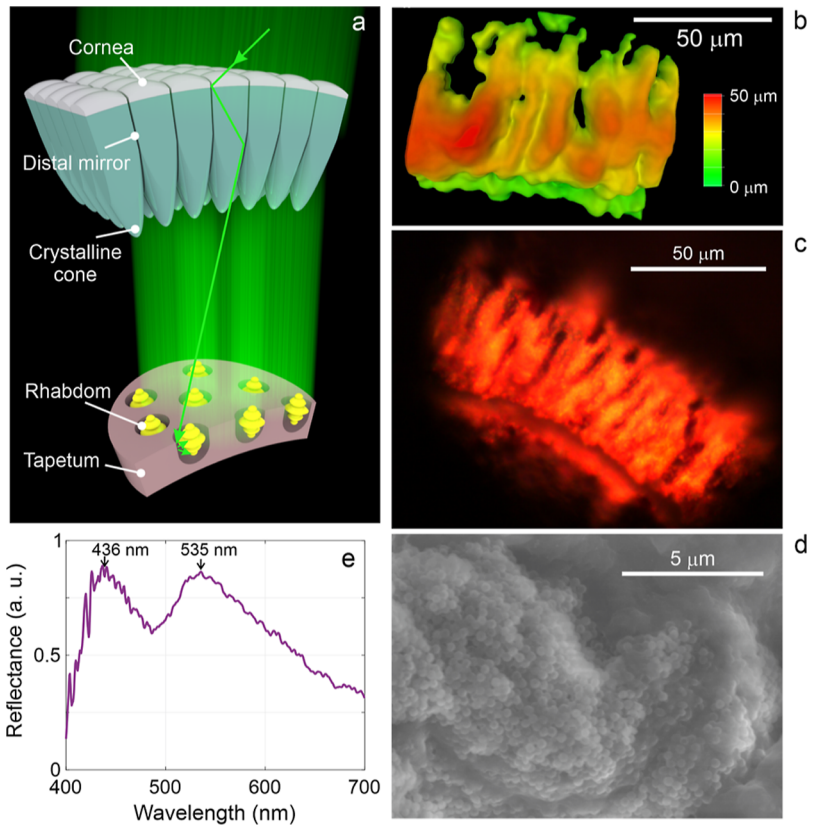

Figure 1. Principle of light collection by a shrimp eye and in situ images of the tapetum cross-section and its reflectance spectrum. (a) Schematic of a shrimp eye showing the ommatidia (square-faceted eye units), rhabdoms (photoreceptive units of the retina), and tapetum reflector (containing arrays of hollow-core isoxanthopterin nanospheres). (b) Confocal topographic and (c) optical microscopy image of the longitudinal tapetum cross-section. The shining effect in (c) is caused by resonant light reflection from arrays of biogenic isoxanthopterin nanoparticles. (d) SEM micrographs of isoxanthopterin nanoparticles on the surface of the tapetum cross-section. (e) Reflection spectrum from the tapetum reflector.

crystal fibers, waveguides, metasurfaces, and high-index Mie resonators.[6,9,10]

Here, we show that an interplay of the isoxanthopterin nanoparticle's radial anisotropy and the interaction between nanoparticles in the array gives rise to a variety of *Q*-BICs in the tapetum of decapod crustaceans. We perform in situ studies of the tapetum for the whiteleg shrimp *Penaeus vannamei* as a model species and discover that its reflection spectrum features pronounced maxima. The comprehensive theoretical study manifests that *Q*-BIC modes lead to not only enhanced reflectivity of the tapetum but also considerably boost the local electromagnetic field. This mechanism of enhancement of light interaction with rhabdoms for the shrimp's tapetum markedly differs from Bragg reflection of other tapetum types. Thus, our findings point to a new BIC-driven mechanism responsible for light collection in eyes of animals.

IN SITU CHARACTERIZATION OF THE TAPETUM REFLECTOR

First, we determine the three-dimensional (3D) organization of the tapetum by confocal microscopy, scanning electron microscopy (SEM), and reflected light optical microscopy, which show membrane-bound elongated protrusions of the tapetal cells enveloping each rhabdom (Figure 1b,c). These structures are typically 5−15 μm wide and 30−100 μm long, and their surfaces are densely packed with biogenic spherical nanoparticles (Figure 1d). Recent studies with cryogenic SEM[3,4] unveiled that the nanoparticles form close-packed 3D assemblies that exhibit a significant short-range order with the periodicity ∼400 nm. This, however, is not observed in Figure 1d since we performed tapetum cutting under the normal ambient conditions and SEM in the environmental regime which did not keep the natural nanoparticles packing. Individual nanospheres possess an average diameter of 330 nm with an onion-like structure: the 70 nm shell is composed of many segments arranged in 8 to 10 concentric lamellae around a hollow core filled with an aqueous medium.[3,4] These segments are nanoscale single-crystal isoxanthopterin plates with dimensions of ca. 50 × 50 × 10 nm. An orthorhombic crystal structure of biogenic isoxanthopterin leads to biaxial optical anisotropy with principal refractive indices of n_a = 1.4, n_b = 2.02, and n_c = 1.9, where "*a*" and "*b*" denote tangential directions along the plate and "*c*" marks the plate normal.[14] Random tangential orientation of the plates inside lamellae allows us to treat the nanoparticle shell as a uniaxial material with an average in-plane ordinary refractive index, n_o = 1.96, and an out-of-plane extraordinary refractive index, n_e = 1.4. Hence, the isoxanthopterin nanoparticles possess a radial-type optical anisotropy with extraordinary and ordinary principal axes pointed toward radial and azimuthal/polar directions (Figure 2a), and their material losses were found to be vanishing in the visible spectral domain.[3]

Next, we perform in situ measurements of the reflection spectra from the tapetum longitudinal cross-section (see the Supporting Information for details). The reflection spectrum

https://doi.org/10.1021/acsphotonics.2c01429
ACS Photonics 2023, 10, 179−184

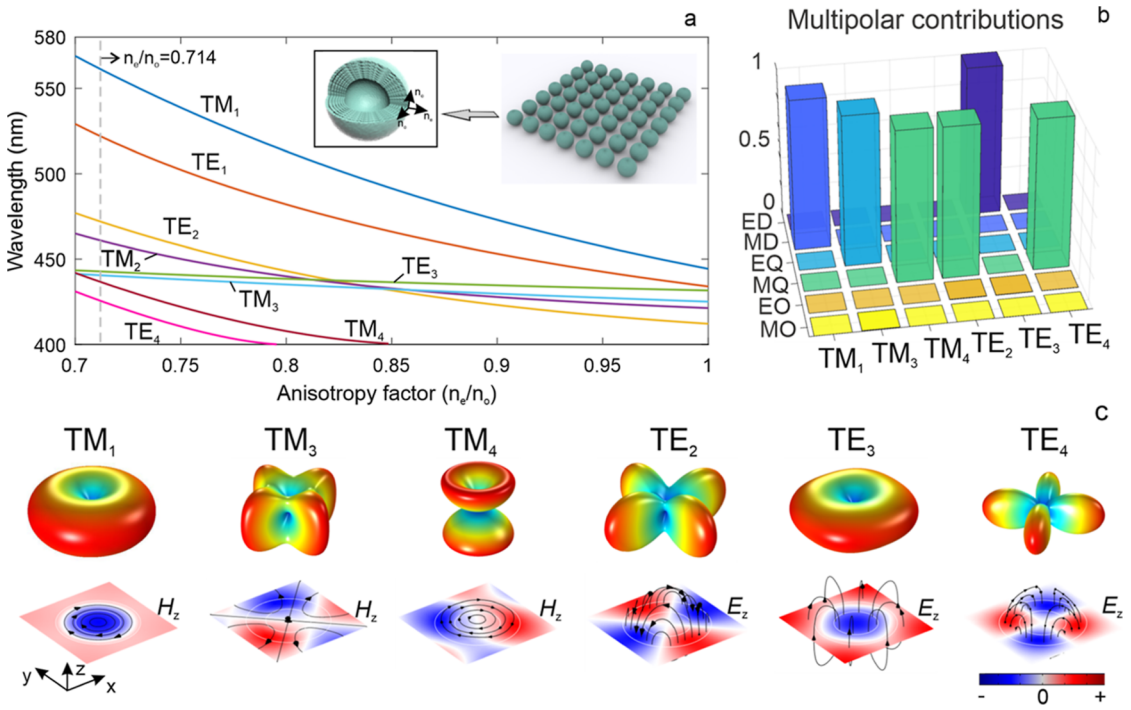

Figure 2. Characterization of bound states in the continuum for the infinite periodic square array of isoxanthopterin core−shell nanoparticles. (a) Wavelengths of the lattice resonances as functions of the anisotropy factor—the ratio of the extraordinary to ordinary refractive index $\eta = n_e/n_o$, obtained by the eigenmode analysis. The inset shows schematics for the lattice and the internal structure of the isoxanthopterin core−shell nanoparticle. The vertical dashed line indicates the anisotropy factor for *L. vannamei* ($n_o = 1.96$ and $n_e = 1.4$). (b) Multipolar expansion for BICs. Cartesian multipoles are denoted as follows: ED, electric dipole; MD, magnetic dipole; EQ, electric quadrupole; MQ, magnetic quadrupole; EO, electric octupole; MO, magnetic octupole. The superposition of all contributions for a given mode is normalized by 1. (c) Radiation patterns and the field structure (H_z and E_z for TM- and TE-polarized BICs, respectively) for the lattice unit cell. Black streamlines denote the electric field **E**.

(Figure 1e) clearly shows two broad maxima at 436 and 535 nm. This fully fits the spectral range where the shrimp's photoreceptors effectively absorb light (between 400 and 550 nm).[15]

THEORETICAL ANALYSIS

To shed light on the physical mechanism behind this phenomenon, we employ finite element modelling (FEM) incorporating all geometrical and material properties of the isoxanthopterin nanoparticles. The 190 nm nanoparticle core is assumed to be filled with a water-like cytoplasm with $n = 1.33$, while the 70 nm shell has a radial isoxanthopterin anisotropy.

We start our theoretical considerations with an eigenmode analysis of an infinite single-layer square array of the isoxanthopterin nanoparticles. To gain insight into the role of the spherical anisotropy, we introduce an anisotropy factor $\eta = n_e/n_o$ and calculate the eigenmode wavelengths of the array at the Γ point as a function of η when $n_e = n_a$ and n_o varies between n_a and n_b (Figure 2a). The anisotropy enhancement results in a significant red shift of eigen wavelengths and expands the spectral band covered by the lattice resonances from 400 to 450 nm in an isotropic case to 430−570 nm for the isoxanthopterin spherical anisotropy (indicated by the dashed vertical line in Figure 2a), which agrees well with the in situ tapetum reflectivity spectrum (Figure 1e).

It is instructive to note that variations in the anisotropy factor may also lead to spectral crossing of the lattice eigenmodes. For example, for the TE_2 and TE_3 modes, it happens at $\eta \sim 0.83$ (Figure 2a). As a result, Fano-type BICs, also known as supercavitation modes, can be formed provided that the modes of the same symmetry are crossed.[16] However, these situations appear for the anisotropy factors lying away from the experimentally discovered value $\eta = 0.714$. Therefore, we do not consider this effect here in detail.

The *Q*-factor analysis (Figure 3d) allows us to distinguish BIC modes, which are TM_1, TM_3, TM_4, TE_2, TE_3, and TE_4. We perform the Cartesian multipolar expansion for those resonances[17−19] and find that every BIC mode contains a single Cartesian multipole (Figure 2b) that stems from the square symmetry of the array. All these BICs also feature radiation absence in the normal direction with respect to the array plane (Figure 2c). This clearly shows the nature of BICs: being embedded into continuum of plane waves normally incident on the lattice, such resonances do not interact with them by reciprocity, forming symmetry-protected BICs.

It is insightful to analyze a transition from true BICs to *Q*-BICs by variations in the light incidence angle (Figure 3a). Figure 3b shows the lattice reflection spectrum as a function of the incidence angle for the TE-polarized wave exciting resonances in the ΓM valley. The reflection maxima positions and linewidths are fully confirmed by the eigenmode dispersions and *Q* factors shown in Figure 3c,d. Non-BIC modes (TE_1 and TM_2) get excited at any incidence angle as their *Q* factors are always finite and comparatively low. In contrast, *Q* factors of BIC modes (TM_1, TE_2, and TM_4) dramatically drop upon deviations of the light incidence angle from 0 that results in excitation of these modes in the reflection spectra. Additionally, one may observe appearance of extra resonances in the reflection at the wavelengths below 460 nm when the incidence angle gets above 0.1 rad. However, they cannot transform into BICs since at the Γ point, their wavelengths drop to the ultraviolet spectral domain where both

https://doi.org/10.1021/acsphotonics.2c01429
ACS Photonics 2023, 10, 179−184

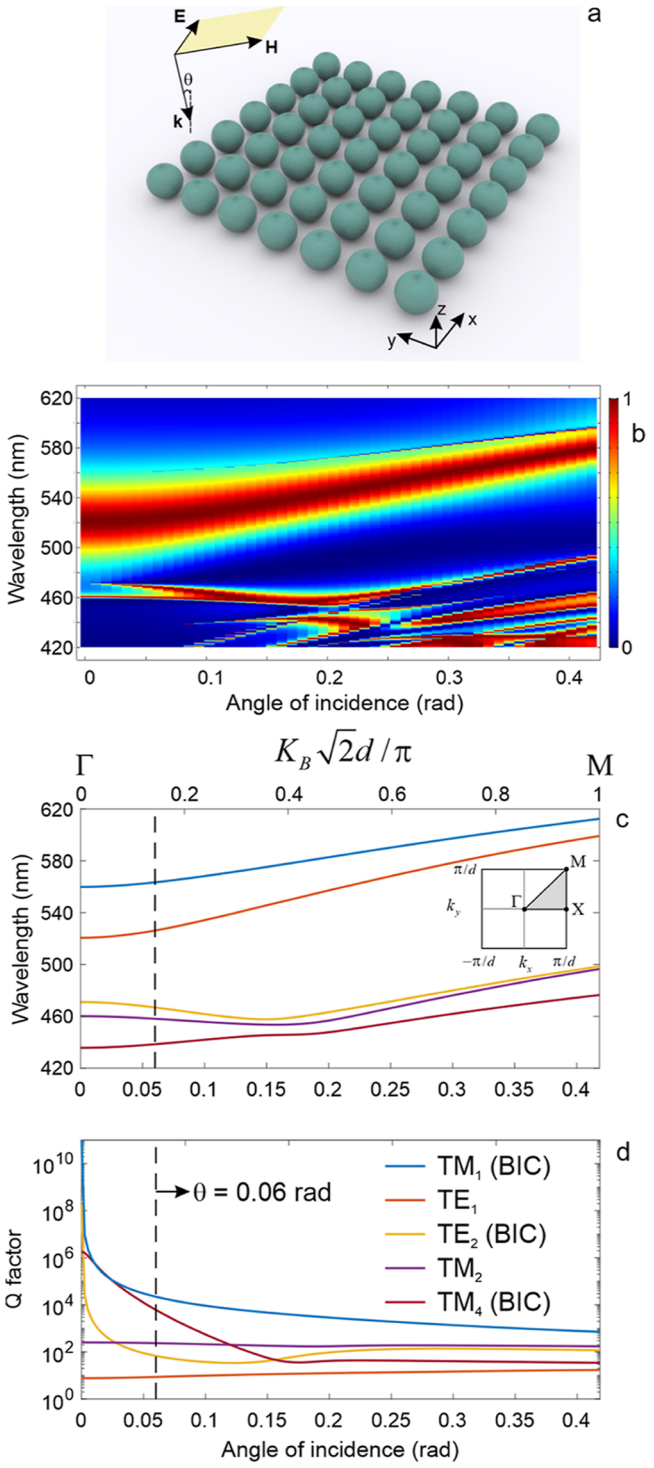

Figure 3. Optical response of the infinite array of isoxanthopterin core−shell nanoparticles. (a) Schematic of the plane wave incident on the lattice. It is considered the case of the lattice excitation in the ΓM valley by the TE-polarized wave that is $\mathbf{E} = \left\{E_0\cos\left(\frac{\pi}{4}\right)\mathbf{x}_0,\ E_0\sin\left(\frac{\pi}{4}\right)\mathbf{y}_0,\ 0\right\}$ and $\mathbf{H} = \left\{H_0\cos\left(\frac{\pi}{4}\right)\cos(\theta)\mathbf{x}_0,\ H_0\sin\left(\frac{\pi}{4}\right)\cos(\theta)\mathbf{y}_0,\ H_0\sin(\theta)\mathbf{z}_0\right\}$. (b) Lattice reflection as a function of the wavelength and the incidence angle. (c) Optical dispersion and (d) Q factors of the array eigenmodes in the ΓM valley. Color encoding for the resonances is the same as in Figure 2. The vertical dashed line denotes the incident angle which was used for simulations shown in Figure 4.

isoxanthopterin and the cellular filling of nanoparticles become opaque.

So far, our analysis has been focused on an infinite array of isoxanthopterin nanoparticles. In order to characterize Q-BICs in a realistic situation, we next analyze their properties upon variations in the array size. Figure 4a shows the spectra of the maximal magnetic field enhancement inside nanoparticles when the array size increases from 2 × 2 to 8 × 8 nanoparticles and the light incidence angle is 0.06 rad. Despite comparatively low refractive indexes of isoxanthopterin, the lattice resonances get well pronounced already for an array of 6 × 6 nanoparticles. Moreover, excitation of Q-BIC resonances in an array of 8 × 8 nanoparticles is accompanied by the magnetic field intensity enhancement exceeding a factor of 100.

Rapid formation of Q-BICs upon growth in the array size is also confirmed by the eigenmode analysis. Figure 4b shows that the dependencies of Q factors for Q-BICs on the array size can be well fitted by the power function n^{α} + const, where n is the total number of nanoparticles in the array and α = 1.3; 1.12; 0.96 for TM$_1$, TM$_4$, and TE$_2$ modes, respectively. Hence, the TM$_1$ mode with a predominant MD contribution and existing already for a 2 × 2 nanoparticles array is best confined and possesses the lowest radiation losses. Being homogeneous in an infinite array, all Q-BIC states transform into lowest-order fundamental lattice resonances reaching the maximal field intensity in the middle of the array (Figure 4e).

It is instructive to compare finite and infinite arrays in terms of reflection and maximal local field enhancement. Figure 4c,d shows that for an infinite array, both Q-BIC and non-BIC resonances appear in both spectra. The situation changes dramatically for an 8 × 8 nanoparticles array. While the spectrum of backward scattering does not have any pronounced spectral features associated with Q-BICs and two comparatively broad maxima correspond to a mix of Q-BIC TE$_2$ and non-BIC TM$_2$ modes as well as to the non-BIC TE$_1$ mode, the spectrum of the local magnetic field enhancement clearly shows the presence of Q-BIC TE$_2$ and TM$_1$ modes. Thus, in relatively small arrays, Q-BIC states come out much stronger in the local field enhancement rather than in the array reflectivity.

Importantly, the results of our numerical model are validated by the in situ reflectivity spectrum of the tapetum cross-section demonstrating two broad maxima located around 436 and 535 nm (Figure 1e), which can be attributed to the mixed TM$_2$ + TE$_2$ and TE$_1$ lattice resonances (Figure 4c), respectively.

CONCLUSIONS AND OUTLOOK

In conclusion, our study shed light on the photonic role of the ordered arrays of radially anisotropic core−shell isoxanthopterin nanoparticles in the tapetum for the whiteleg shrimp *P. vannamei*. Such a tapetum structure gives rise to a variety of Q-BIC lattice resonances associated with the enhancement of the tapetum reflectivity and the local electromagnetic field in a wideband visible domain from blue to green light. We find that for Q-BICs, the local field boosting is much more immune to shrinking the array size than the tapetum reflectivity. Taking into account that previous in situ studies of the tapetum showed that isoxanthopterin nanoparticles are typically packed into small periodic ensembles,[3,4] one may conclude that the key biological function of Q-BIC states is the boosting of the local optical field which eventually read out by rhabdoms through some mechanism that is yet to be discovered. We may

https://doi.org/10.1021/acsphotonics.2c01429
ACS Photonics 2023, 10, 179−184

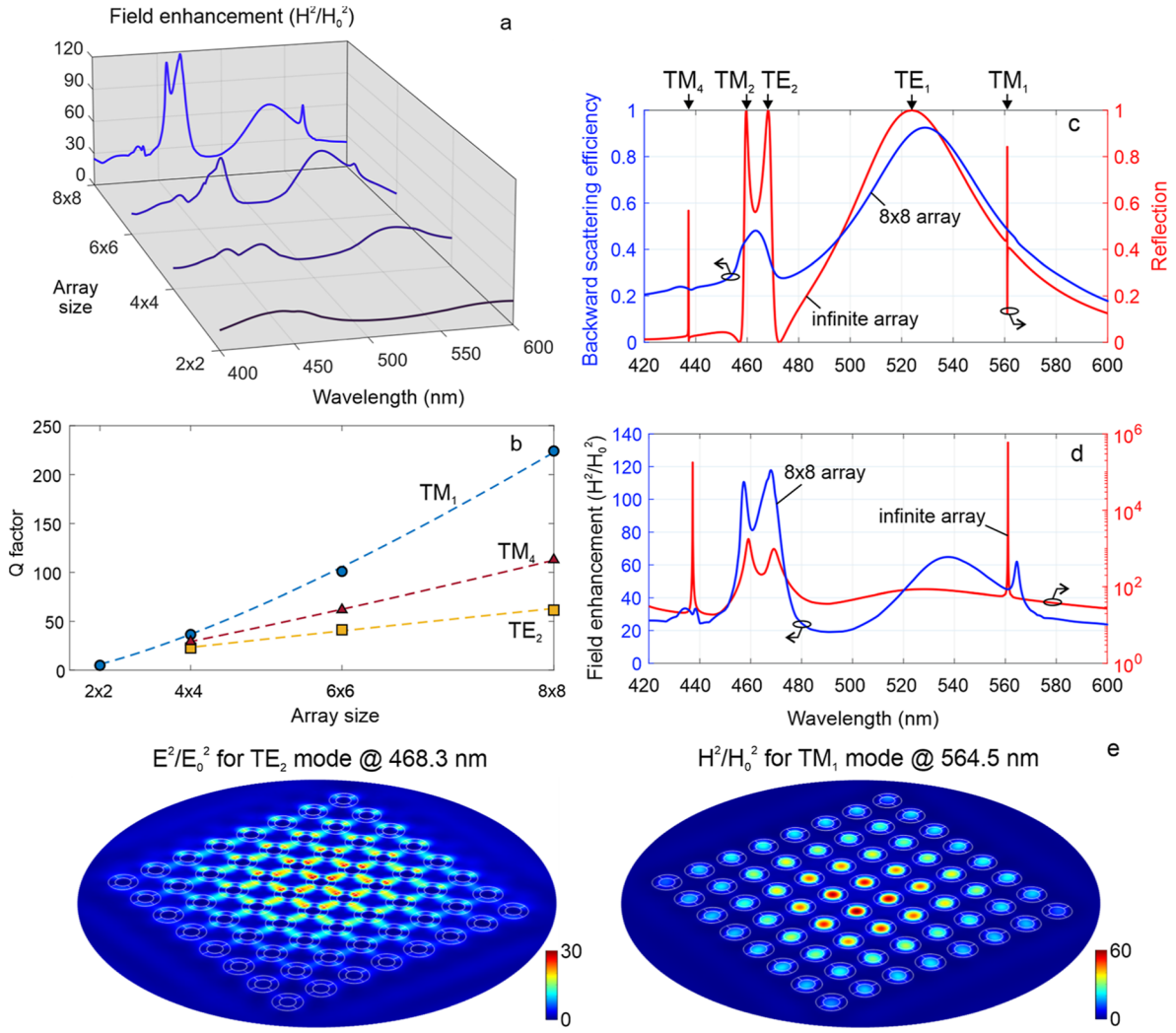

Figure 4. Comparison of Q-BICs in the infinite and finite lattices. (a) Spectra of the maximal magnetic field enhancement and (b) Q factor of Q-BICs for finite arrays of 2 × 2, 4 × 4, 6 × 6, and 8 × 8 nanoparticles. (c) Backward scattering efficiency and reflection and (d) maximal magnetic field enhancement for the 8 × 8 nanoparticles and infinite array, respectively. (e) Field structure for TE_2 and TM_1Q-BICs excited in the array of 8 × 8 nanoparticles. In all simulations, θ = 0.06 rad.

speculate that this mechanism can be based on the near-field energy transfer.

Our findings suggest that the pteridine isoxanthopterin can serve as a promising platform for the next-generation biophotonic nanodevices as it allows the synthesis of nanostructures with specific symmetries able to realize non-trivial light−matter interactions resulting in numerous applications, spanning from bioimaging to biosensing.[20−22] For example, heating-free quasi-BIC resonances tunable in the full optical domain open opportunities for quenching-free enhancement of luminescence from the attached emitters (such as dyes or proteins).

■ ASSOCIATED CONTENT

Supporting Information

The Supporting Information is available free of charge at https://pubs.acs.org/doi/10.1021/acsphotonics.2c01429.

Additional experimental details on samples preparation and in situ measurements (PDF)

■ AUTHOR INFORMATION

Corresponding Author

Roman E. Noskov − *Department of Electrical Engineering, Tel Aviv University, Tel Aviv 69978, Israel; Light-Matter Interaction Centre, Tel Aviv University, Tel Aviv 69978, Israel; Integrated Photonics Technologies Research Unit, Microsystems Division, Silicon Austria Labs GmbH, High Tech Campus Villach, Villach 9524, Austria;* orcid.org/0000-0002-9752-8527; Email: roman.noskov@silicon-austria.com

Authors

Andrey Machnev − *Department of Electrical Engineering, Tel Aviv University, Tel Aviv 69978, Israel; Light-Matter Interaction Centre, Tel Aviv University, Tel Aviv 69978, Israel*

Daniel Ofer − *Department of Electrical Engineering, Tel Aviv University, Tel Aviv 69978, Israel; Light-Matter Interaction Centre, Tel Aviv University, Tel Aviv 69978, Israel*

Hod Gilad − *Department of Electrical Engineering, Tel Aviv University, Tel Aviv 69978, Israel; Light-Matter Interaction Centre, Tel Aviv University, Tel Aviv 69978, Israel*

https://doi.org/10.1021/acsphotonics.2c01429
ACS Photonics 2023, 10, 179−184

Jenia Binenbaum − *School of Plant Sciences and Food Security, Tel Aviv University, Tel Aviv 69978, Israel;* orcid.org/0000-0003-4724-3563
Lior Schneidman − *School of Plant Sciences and Food Security, Tel Aviv University, Tel Aviv 69978, Israel*
Ya'arit Levitt-Barmats − *The Steinhardt Museum of Natural History, Israel National Center for Biodiversity Studies, Tel Aviv University, Tel Aviv 69978, Israel*
Pavel Ginzburg − *Department of Electrical Engineering, Tel Aviv University, Tel Aviv 69978, Israel; Light-Matter Interaction Centre, Tel Aviv University, Tel Aviv 69978, Israel*

Complete contact information is available at: https://pubs.acs.org/10.1021/acsphotonics.2c01429

Notes

The authors declare no competing financial interest.

■ ACKNOWLEDGMENTS

The authors are grateful to AquaMoaf Shrimp R&D Center (Israel) for supplying alive shrimps and to the Steinhardt Museum of Natural History, Israel National Center for Biodiversity Studies, Tel Aviv University.

■ REFERENCES

(1) Palmer, B. A.; Gur, D.; Weiner, S.; Addadi, L.; Oron, D. The Organic Crystalline Materials of Vision: Structure-Function Considerations from the Nanometer to the Millimeter Scale. *Adv. Mater.* **2018**, *30*, 1800006.
(2) Land, M. F. Eyes with Mirror Optics. *J. Opt. A: Pure Appl. Opt.* **2000**, *2*, R44−R50.
(3) Palmer, B. A.; Hirsch, A.; Brumfeld, V.; Aflalo, E. D.; Pinkas, I.; Sagi, A.; Rosenne, S.; Oron, D.; Leiserowitz, L.; Kronik, L.; Weiner, S.; Addadi, L. Optically Functional Isoxanthopterin Crystals in the Mirrored Eyes of Decapod Crustaceans. *Proc. Natl. Acad. Sci.* **2018**, *115*, 2299−2304.
(4) Palmer, B. A.; Yallapragada, V. J.; Schiffmann, N.; Wormser, E. M.; Elad, N.; Aflalo, E. D.; Sagi, A.; Weiner, S.; Addadi, L.; Oron, D. A Highly Reflective Biogenic Photonic Material from Core−Shell Birefringent Nanoparticles. *Nat. Nanotechnol.* **2020**, *15*, 138−144.
(5) von Neumann, J.; Wigner, E.Über merkwürdige diskrete Eigenwerte. *The Collected Works of Eugene Paul Wigner*; Springer Berlin Heidelberg, 1993; Vol, *30*, p 291.
(6) Hsu, C. W.; Zhen, B.; Stone, A. D.; Joannopoulos, J. D.; Soljačić, M. Bound States in the Continuum. *Nat. Rev. Mater.* **2016**, *1*, 16048.
(7) Marinica, D. C.; Borisov, A. G.; Shabanov, S. V. Bound States in the Continuum in Photonics. *Phys. Rev. Lett.* **2008**, *100*, 183902.
(8) Bulgakov, E. N.; Sadreev, A. F. Bound States in the Continuum in Photonic Waveguides Inspired by Defects. *Phys. Rev. B: Condens. Matter Mater. Phys.* **2008**, *78*, 075105.
(9) Azzam, S. I.; Kildishev, A. V. Photonic Bound States in the Continuum: From Basics to Applications. *Adv. Opt. Mater.* **2021**, *9*, 2001469.
(10) Joseph, S.; Pandey, S.; Sarkar, S.; Joseph, J. Bound States in the Continuum in Resonant Nanostructures: An Overview of Engineered Materials for Tailored Applications. *Nanophotonics* **2021**, *10*, 4175−4207.
(11) Ndangali, R. F.; Shabanov, S. V. Electromagnetic Bound States in the Radiation Continuum for Periodic Double Arrays of Subwavelength Dielectric Cylinders. *J. Math. Phys.* **2010**, *51*, 102901.
(12) Hsu, C. W.; Zhen, B.; Lee, J.; Chua, S.-L.; Johnson, S. G.; Joannopoulos, J. D.; Soljačić, M. Observation of Trapped Light within the Radiation Continuum. *Nature* **2013**, *499*, 188−191.
(13) Koshelev, K.; Lepeshov, S.; Liu, M.; Bogdanov, A.; Kivshar, Y. Asymmetric Metasurfaces with High- Q Resonances Governed by Bound States in the Continuum. *Phys. Rev. Lett.* **2018**, *121*, 193903.
(14) Hirsch, A.; Palmer, B. A.; Ramasubramaniam, A.; Williams, P. A.; Harris, K. D. M.; Pokroy, B.; Weiner, S.; Addadi, L.; Leiserowitz, L.; Kronik, L. Structure and Morphology of Light-Reflecting Synthetic and Biogenic Polymorphs of Isoxanthopterin: A Comparison. *Chem. Mater.* **2019**, *31*, 4479−4489.
(15) Matsuda, K.; Wilder, M. N. Difference in Light Perception Capability and Spectral Response between Juveniles and Sub-Adults of the Whiteleg Shrimp Litopenaeus Vannamei as Determined by Electroretinogram. *Fish. Sci.* **2010**, *76*, 633−641.
(16) Rybin, M. V.; Koshelev, K. L.; Sadrieva, Z. F.; Samusev, K. B.; Bogdanov, A. A.; Limonov, M. F.; Kivshar, Y. S. High-Q Supercavity Modes in Subwavelength Dielectric Resonators. *Phys. Rev. Lett.* **2017**, *119*, 243901.
(17) Terekhov, P. D.; Baryshnikova, K. V.; Artemyev, Y. A.; Karabchevsky, A.; Shalin, A. S.; Evlyukhin, A. B. Multipolar Response of Nonspherical Silicon Nanoparticles in the Visible and Near-Infrared Spectral Ranges. *Phys. Rev. B* **2017**, *96*, 035443.
(18) Barhom, H.; Machnev, A. A.; Noskov, R. E.; Goncharenko, A.; Gurvitz, E. A.; Timin, A. S.; Shkoldin, V. A.; Koniakhin, S. V.; Koval, O. Yu.; Zyuzin, M. V.; Shalin, A. S.; Shishkin, I. I.; Ginzburg, P. Biological Kerker Effect Boosts Light Collection Efficiency in Plants. *Nano Lett.* **2019**, *19*, 7062−7071.
(19) Noskov, R. E.; Machnev, A.; Shishkin, I. I.; Novoselova, M. V.; Gayer, A. V.; Ezhov, A. A.; Shirshin, E. A.; German, S. V.; Rukhlenko, I. D.; Fleming, S.; Khlebtsov, B. N.; Gorin, D. A.; Ginzburg, P. Golden Vaterite as a Mesoscopic Metamaterial for Biophotonic Applications. *Adv. Mater.* **2021**, *33*, 2008484.
(20) Humar, M.; Kwok, S. J. J.; Choi, M.; Yetisen, A. K.; Cho, S.; Yun, S.-H. Toward Biomaterial-Based Implantable Photonic Devices. *Nanophotonics* **2017**, *6*, 414−434.
(21) Pan, T.; Lu, D.; Xin, H.; Li, B. Biophotonic Probes for Bio-Detection and Imaging. *Light Sci. Appl.* **2021**, *10*, 124.
(22) Vickerman, B. M.; Zywot, E. M.; Tarrant, T. K.; Lawrence, D. S. Taking Phototherapeutics from Concept to Clinical Launch. *Nat. Rev. Chem* **2021**, *5*, 816−834.